Trans Indian Inst Met
https://doi.org/10.1007/s12666-020-01880-5

ORIGINAL ARTICLE

Investigating the Failure of Exhaust Impeller Fan Blades of Indurating Machines in Iron Ore Pelletizing Plant: Effective Solutions for Improvements

Mehdi Alizadeh[1] · Mahdi Kiani Khouzani[1] · Mohsen Alizadeh[2]

Received: 15 June 2019 / Accepted: 17 January 2020

Abstract In essence, when steel industry in concerned, facing the destructive parameters is inevitable, specifically in pelletizing plant, where the indurating machine is severely damaged. A similar fortune is considerable for the impeller fan blades of the exhaust systems in such arrangements in industry. Austempering heat treatment is a cheap and easy process to improve the service life of the items by enhancing the mechanical properties and, of course, wear resistance. This work is part of a broader program concerning optimizing process conditions and applying possible improvements to enhance the service life for each individual item in the steel industry. In this research, it was focused on impeller fan blades, where a new chemistry was employed to casting operation by the addition of specified amounts of nickel, molybdenum and copper to chemical composition of the ductile cast iron GGG60. The produced samples were subjected to austempering process at a predicted time and temperature in a salt bath. A range of techniques were employed to study the mechanical properties and assess the wear behavior of the samples. The findings showed that the acicular ferrite was formed by the austempering process, leading to the enhancement of wear resistance and consequently improving the performance of the impeller blades. This improvement was also verified by simulation employing ABAQUS and SolidWorks software. The latter was to confirm the actual performance of the impeller fan blade, whereas the alloy sufferred from reduction in elongation during austempering process.

Keywords Impeller fan blades · Ductile cast iron · Wear properties · Casting · Heat treatment · Simulation

✉ Mehdi Alizadeh
alizadeh@cc.iut.ac.ir

[1] Department of Materials Engineering, Isfahan University of Technology, Isfahan 84156 83111, Iran

[2] Research Institute for Steel, Isfahan University of Technology, Isfahan 84156 83111, Iran

1 Introduction

Principally, during the iron ore pelletizing process, an aqueous mixture of raw materials including fine iron ore concentrate, binding agents (bentonite) and fluxes (limestone, olivine and dolomite) is provided and pulped in a sloped pelletizing ball disk to form a green pellet formed with 9–16 mm size. In order to increase the compression strength, green pellet is heated above 1300 °C for a few minutes. In this process, moisture and dust are transferred to the process gas and further to the heating cycle of green pellet that are vacuum pumped by the impeller of fan. Figure 1 shows a schematic overview of impeller blade location. An impeller is a rotor that increases flow of the fluid or gas by raising a specified volume of the flow to a specified pressure level. In the exhausted gases, there are abrasive and corrosive materials, e.g., dust particles, sulfur gas and moisture. Due to the presence of destructive factors in the fan environment, the blades eventually suffer from severe surface damages (see Fig. 2) and need to be urgently replaced. Repairs and replacements in short intervals, manufacturing line stops, and increased repair costs and consumable parts result in the reduced productivity of the pelletizing plant. Erosion/wear owing to moisture in low-pressure blades has remained as concern and problem throughout steam turbine history [1–7].

Erosion, as a type of wear, is the progressive loss of solid surface of original material due to a mechanical

Published online: 14 February 2020

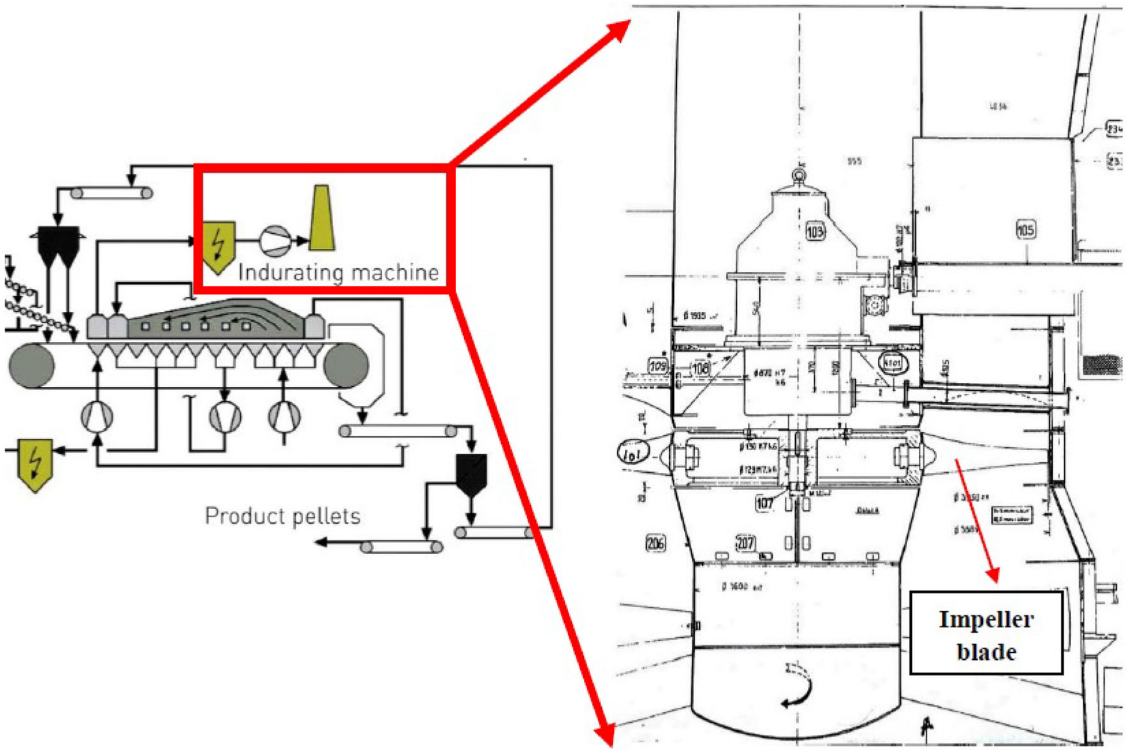

Fig. 1 Schematic view of indurating machine and impeller blade showing failed section

interaction between impinging solid or liquid particles, a multicomponent fluid and the surface. In fact, erosion can be categorized into two specific terms: solid particle erosion and liquid impingement erosion. Impacts by liquid drops lead to liquid impingement erosion. Cavitation is the removal of material surface by the vapor and gas bubble formation due to the sudden reduction in fluid pressure and rapid collapse of bubbles, caused by increment of fluid pressure in the downstream. Cavitation prevalently occurs in hydraulic systems, pumps, turbine bearings, valves, etc. Cavitation–erosion is a type of surface failure by microjet, shock waves or the mechanical process of material removal owing to the vapor bubble collapse (implosion) [7–10]. In case of impeller blades, there is an efficient and suitable approach of surface modification processes available such as nitrogenating, boron coating or other thermal spraying methods. However, due to the high cost of the methods for large industrial parts, they are not economically favorable approaches. Meanwhile, applying erosion-resistant overlays cannot protect many small areas. Therefore, providing a better alternative seems to be vital, when erosion-resistant metal is available, which has reasonable hardness. Perhaps, applying specific types of posttreatment is a key trick to overcome the challenges faced in the industry. Austempering heat treatment process is a lenient approach for increasing wear resistance (or erosion) and corrosion of ductile cast iron. Nowadays, austempered ductile iron (ADI) casting is in competition with alloying and hard facing steel. Austempering is a process which creates a bainite matrix that increases the abrasion resistance, corrosion resistance and yield strength without loss of impact resistance [11–14]. This process involves heating the alloy in the austenite area (about 870 to 900 °C) and then placing it in a salt bath at a constant temperature (between 220 and 400 °C) and in the ordinary cold water. Zimba et al. examined the effect of austempering process on the resistance to abrasion of ductile iron [15–17]. They observed that the presence of bainite with carbide as well as the residual austenite, formed during the austempering process, leads to an increase in the wear resistance of the alloy. The residual austenite is transformed into martensitic, under the load of the abrasion medium, increasing the wear resistance.

As known, ADI cast iron is widely used due to its stable microstructure in many industrial equipments including gears, high-abrasion-resistant parts, automobile crankcase and refrigerator compressors. In order to design metals with both good mechanical properties and high wear resistance, strong carbide-forming addition is a well-known approach [18]. In order to modify the service life of wear-resistant parts in iron ore pelletizing plant, a ductile cast iron is made, improved by carbides. Nickel improves the ultimate tensile strength (UTS) without any effect on the impact toughness value, also increases residual austenite and as a result improves hardenability. Molybdenum also increases hardenability and also creates abrasion-resistant particles (molybdenum carbide). The addition of Cu to cast iron causes transformation from ferrite matrix to a pearlite matrix that significantly improves the mechanical properties, especially hardness as well as wear resistance [19, 20].

Having mentioned the benefits of ADI and challenges facing the industry in different aspects, it seems to be necessary to study the failure of the devices made by ADI cast irons. Considering the spirit of development and industrial approach, this work has been presented, in which failure of the impeller was investigated and the effects of austempering process as well as optimizing the chemistry were assessed. Meanwhile, the abrasive behavior and mechanical properties of ductile cast iron were also studied in detail. Eventually, simulation methods were performed in order to ensure the proper performance of fan impeller in its working condition with new properties due to the additional element alloying and heat treatment process.

2 Experimental

The specifications of the impeller fan, used in the pelletizing plant, are presented in Table 1. The chemical composition of the failed impeller (ductile cast iron GGG60) and alloying cast iron is given in Table 2. In order to apply austempering process, the specimens were austenised at 900 °C for 90 min in an electric furnace with a heating rate of 3 °C/s. Then, the specimens were austempered for 120 min in a salt bath oven at various temperatures. An alloy with the properties similar to the one given in Table 2 was provided and casted in Y-shaped blocks (dimensions $35 \times 18 \times 4$ cm^3). In order to investigate the microstructure of the cast iron, the specimen was subjected to etching process in Nital 2% solution. In order to evaluate the wear behavior, the standard pin-on-disk test was carried out based on ASTM G-99, under 12 kg load at the room temperature. Hardness was assessed employing Brinell method under 187.5 N load and 2.5-mm-diameter steel ball for 20 s. The tensile test was carried out at room temperature with a pulling speed of 4 mm/min; also, Charpy test for impact toughness measuring was performed (without notch). The scanning electron microscopy (SEM) (Philips, XL 30), together with energy-dispersive X-ray spectroscopy (EDS), was employed to study the worn surface. The modeling section was carried out based on the finite element analysis of fan blades using the ABAQUS 6.14 software. SolidWorks software was also used to model the components. Due to the large volume of the issue, the simulation was performed using a powerful computer with eight processor cores and 16 GB of RAM. The modeling analysis was for the sake of assurance of maximum mechanical properties (including ultimate strength and flexibility).

3 Results and Discussion

3.1 Visual Observation

Figure 2 shows a macroscopic image of failed impeller and macroscopic images of impeller surface. There are no signs of excessive deformation and corrosion products from visual inspection.

Table 1 shows that in the working atmosphere of the fan, there is sulfur dioxide derived from fossil fuels, which is one of the main destructive parameters in the industry.

Sulfur dioxide exposed to moisture can lead to the production of sulfuric acid (There is some moisture in the iron ore green pellet.). However, ductile iron exposed to sulfuric acid has a corrosion rate of about 0.2 mm/year, while the typical steel has a corrosion rate of 2.5 mm/year [19]. Another important issue is the dew formation and dew point temperature. At temperatures below the dew point, the gas begins to form liquid droplets on the metal; when it happens on a surface surrounded with an environment, which contains sulfur, there is a possibility of sulfuric acid to be formed; therefore, corrosion occurs in the impeller. In the working environment, the moisture content is about 4.5% and SO_2 concentration is about 210 ppm, and the maximum dew point temperature in these conditions is about 130 °C [20]. The temperature of the working area is around 150 °C, when the fan operates at a normal condition. Therefore, the chance of dew formation on impeller blades is low and corrosion of impellers is not a major failure mechanism.

As shown in Fig. 2a, cavity is created on the surface of the blade. The cavities are on the surface and at an angle to the surface normal. Also, these cavities are not visible on

Table 1 Technical specification of fan impeller blades (taken from the laboratory of the company)

Type of materials	Rate (rpm)	O_2 (%)	NO (ppm)	SO_2 (ppm)	Moisture (%)	Working temperature (°C)
GGG60	435	18	258	210	4.5	150

Table 2 Chemical composition of failed impeller fan and alloying cast iron

Elements	C	Mn	P	S	Si	Cr	Mo	Ni	Cu
Failed specimen	3.50	0.40	0.08	0.02	2.70	0.02	0.10	0.30	0.10
Alloying cast iron	3.56	0.13	0.03	0.01	2.21	0.35	0.30	1.10	0.73

the ready-made blades. Since the temperature of place prevents dew formation on the blade and these cavities are only formed on the surface, the cavities can be linked to the damaging erosion-–cavitation mechanism due to the presence of dust and solid particles in the fan atmosphere [21].

Figure 2b and c shows an overview of the impeller surface. As can be seen, ragged grit blast and the pits are horseshoe-shaped (owing to impingement of solid particles) with some cavities or pits (white arrow) due to cavitation appearing at the surface of impeller; all the evidences indicate the erosion–cavitation mechanism; therefore, erosion is a major failure mechanism.

In addition, it is known that the cavities are formed at an angle of about 20 to 30 degrees relative to the horizontal axis, due to the geometric shape of the blades of the impeller. The erosion of the ductile materials highly

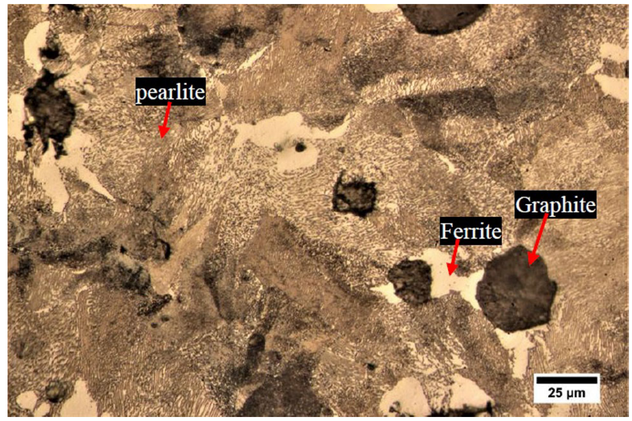

Fig. 3 OM microstructure of the failed fan impeller

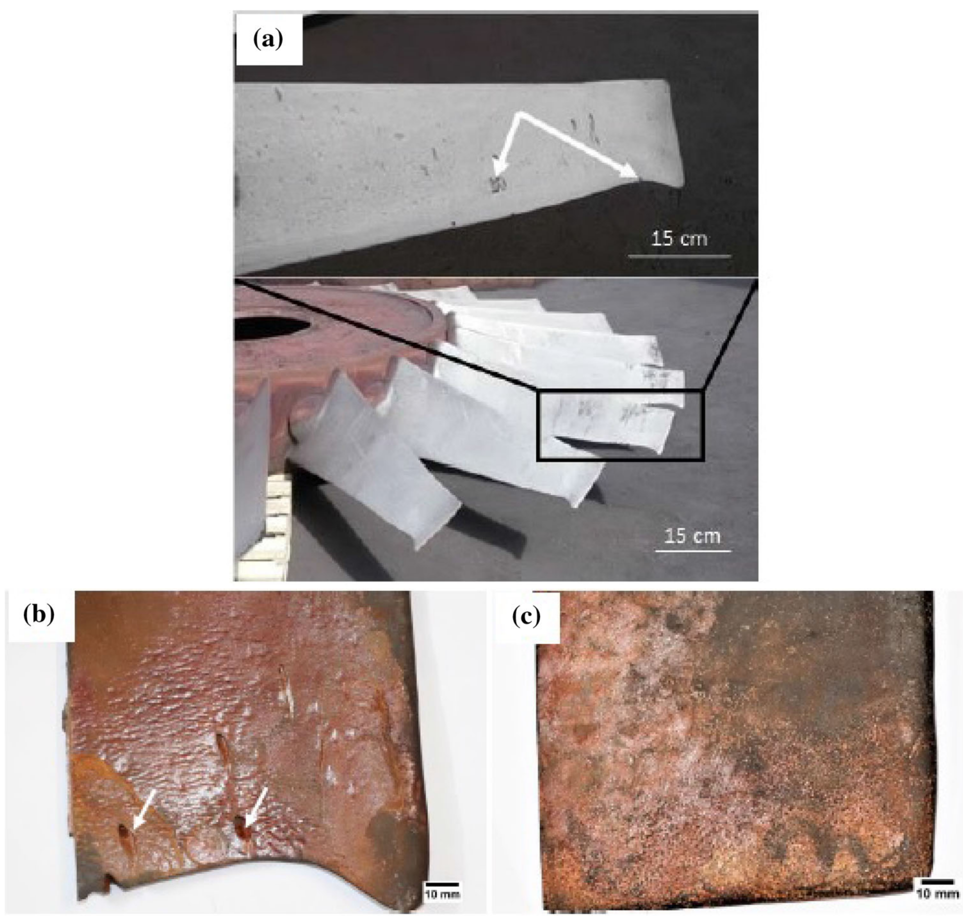

Fig. 2 Overview of failed impeller and its surface (corrosion products shown in **b** and **c** are from failed specimens in the warehouse not in its working conditions)

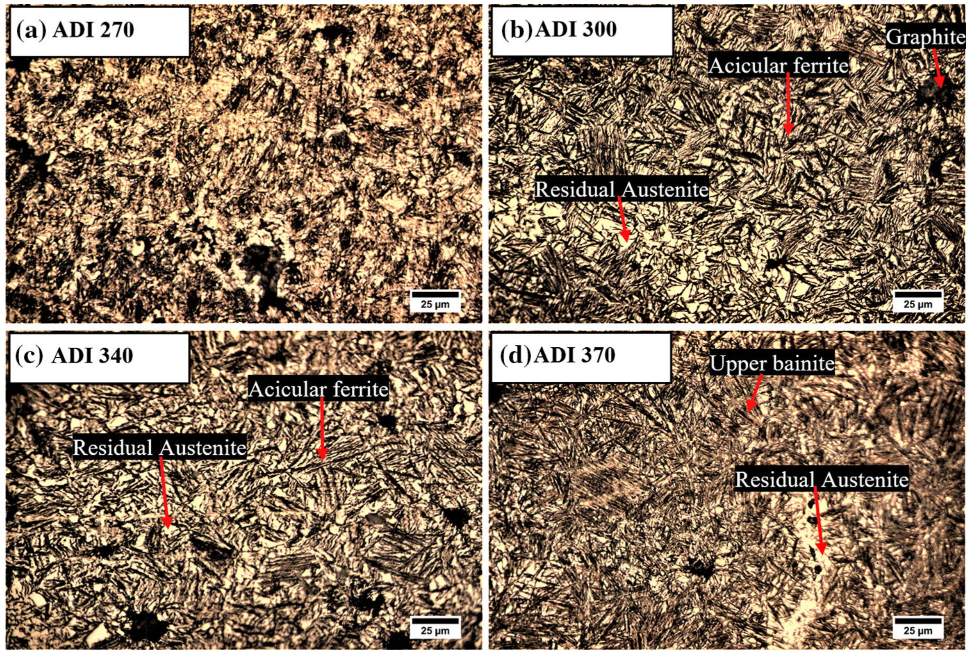

Fig. 4 OM microstructure of primary ductile cast iron after austempered at **a** 270 °C, **b** 300 °C, **c** 340 °C, **d** 370 °C

depends on the angle of the collision of particles, and usually, the maximum erosion occurs at an angle between 20° and 30° [22]. The collision of particles under a tilted angle causes the plastic formation along with removal of material from the surface, which is shown in Fig. 2.

Of course, this assumption is true when the hardness of abrasive particles is approximately 1.2 times higher than the surface hardness [23]. The abrasive particles are mainly magnetite iron ore that has a hardness of about 500 HV and hardness of a typical ductile cast iron 200 HV; hence, the assumption is valid.

The presence of these particles and their collision with ductile cast iron leads to the removal of graphite from the surface and increases stress concentration. By creating these empty holes of graphite and the collision of particles, these cavities grow and the impeller fracture occurs [21]. Consequently, a matrix seems to be responsible to resist against the plastic deformation, and therefore, it can improve wear/erosion resistance up to a considerable level.

3.2 Microstructure and Hardness

Figure 3 shows microstructure of a failed impeller. It is observed that the impeller blade is made of ductile cast iron with 100% ledeburite and almost perlite microstructure.

The graphite morphology of cast iron is based on ASTM A247 standard in groups I and II. The number of nodules (spherical graphite) for this cast iron is approximately 221 per millimeter square. In addition, due to the fact that the microstructure is completely pearlite, it is known that the molten is casted after cooling in air only without being subjected to various heat treatment processes such as annealing or austempering.

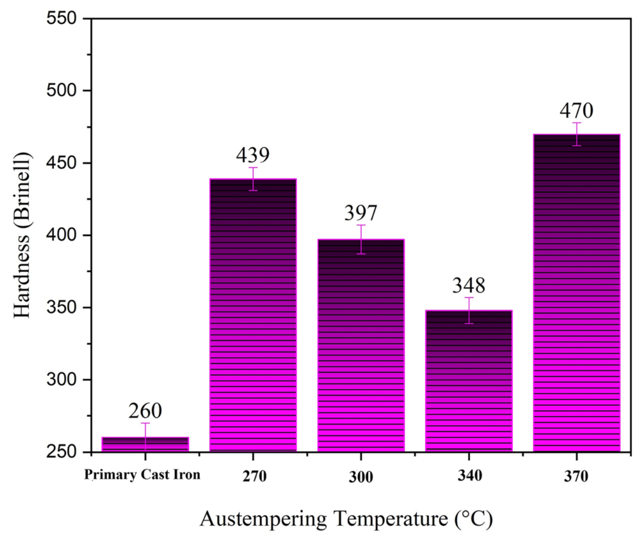

Fig. 5 Hardness variation with austempering temperature (°C)

Figure 4 shows the microstructure of ductile cast iron after austenitizing at 900° C for 90 min and austempering at different temperatures. It can be seen that the matrix of cast iron austempered at 270 °C (ADI270) contains lower bainite (acicular ferrite) with small amount of martensite without any residual austenite. By placing austenitic cast iron in the salt bath, the ferrite begins to nucleate and the carbon returns to adjacent areas. In the ADI 270 sample, due to the low process temperature, carbon slightly diffuses into the austenitic zones. Therefore, when the sample is taken out of the salt bath, the formed austenite is unstable, and therefore, it is converted to martensitic. As a result, the microstructure of the residual austenite is not observed and the matrix consists of acicular ferrites (lower bainite) and martensite [22–24]. Figure 4b shows that the acicular ferrite is grown by increasing the austempering temperature and also the residual austenite (bright areas) is formed. An increase in the austempering temperature, in case of the ADI300 sample, causes depletion and increase in diffusion of carbon from ferrite, and therefore, carbon-rich austenitic zones are formed [21]. The combination of the ferrite and residual austenite, in the microstructure, is called ausferrite, which enhances mechanical properties of austempered ductile cast iron [18].

In the ADI340 sample, it is observed that the residual austenite is significantly increased and a thick acicular ferrite is created (Fig. 4c). By increasing the austempering temperature to 370° C of the ADI 370 sample, the acicular ferrite transforms to upper bainite [17].

On the other hand, by increasing the temperature of the austempering to 370 °C, the acicular ferrite becomes longer and thicker. Hence, acicular ferrite transforms to upper bainite and the austenite crystals distribute between packets of upper bainite [24]. Obviously, at high austempering temperatures, due to the fact that the acicular ferrite clusters are not parallel together, they seem similar to the upper bainite.

The ductile cast iron hardness variations with austempering temperature are shown in Fig. 5 to be compared with non-heat-treated specimen. The low hardness of the primary specimen is due to its ferrite–perlite microstructure. As it is known, the hardness of the austempered specimen at 270° C has been strongly increased compared to the raw specimen. Increasing the hardness of

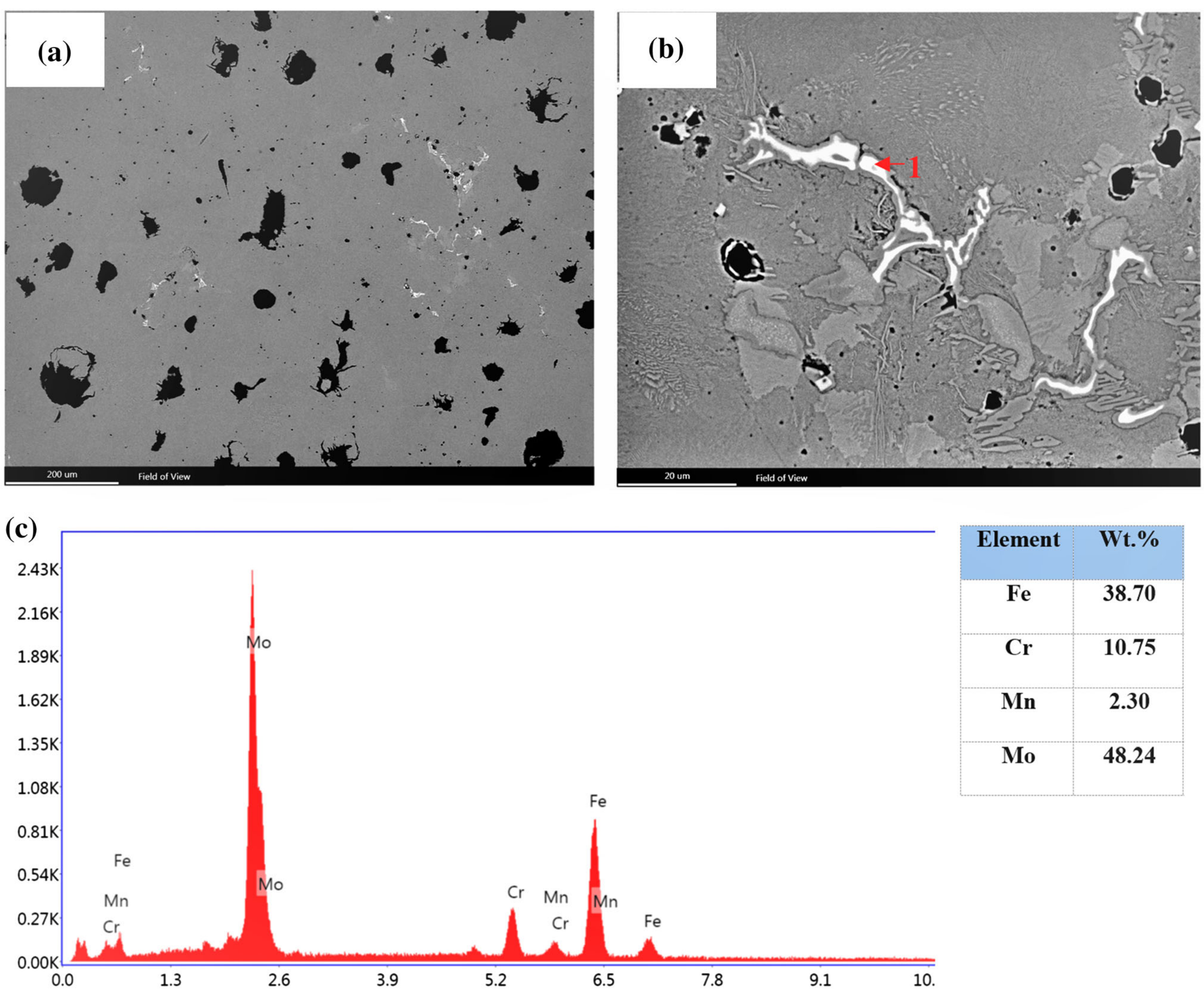

Element	Wt.%
Fe	38.70
Cr	10.75
Mn	2.30
Mo	48.24

Fig. 6 **a** and **b** SEM (BSE) image of microstructure of alloying cast iron; **c** EDS point analyses, taken from the marked spot, shown in (**b**)

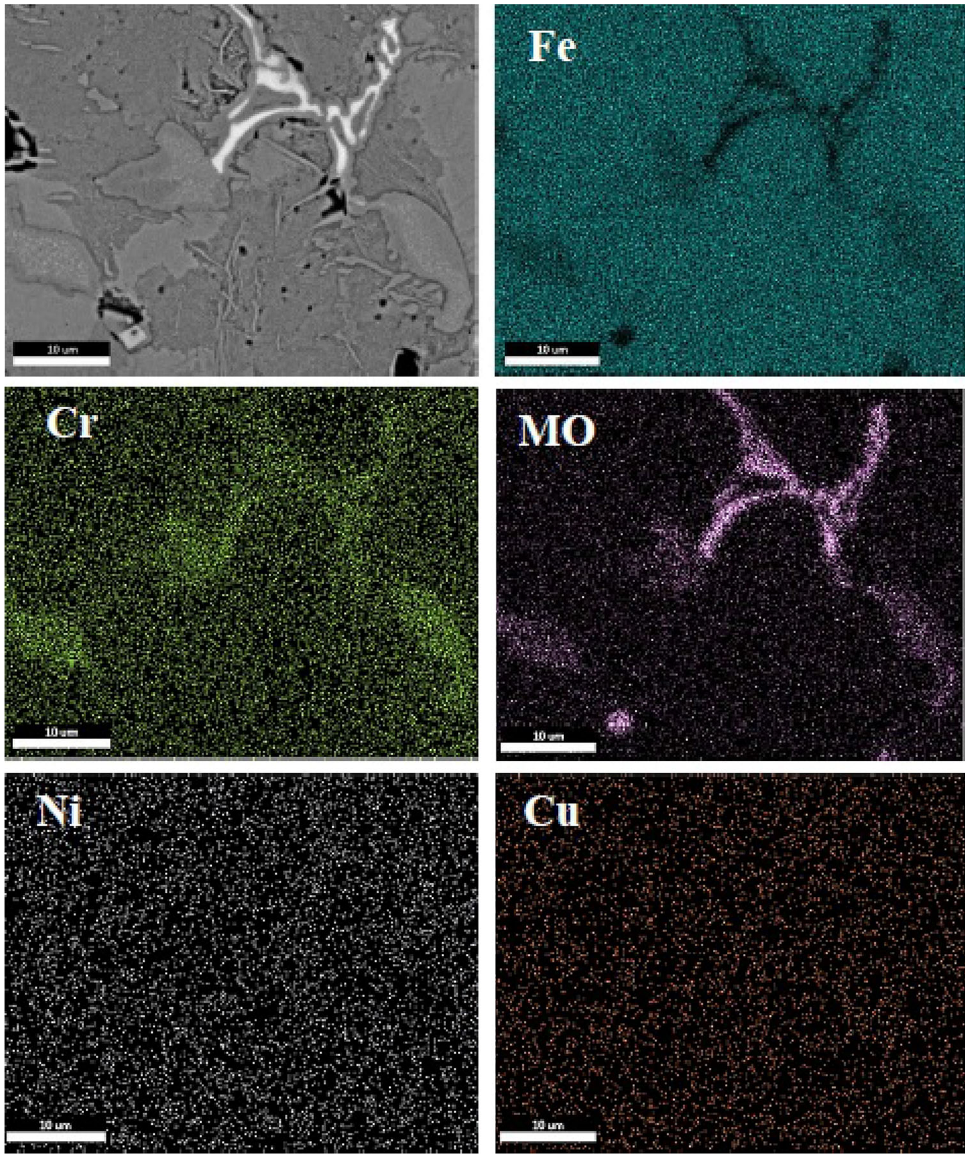

Fig. 7 Elemental mapping analysis from the alloying ductile cast iron

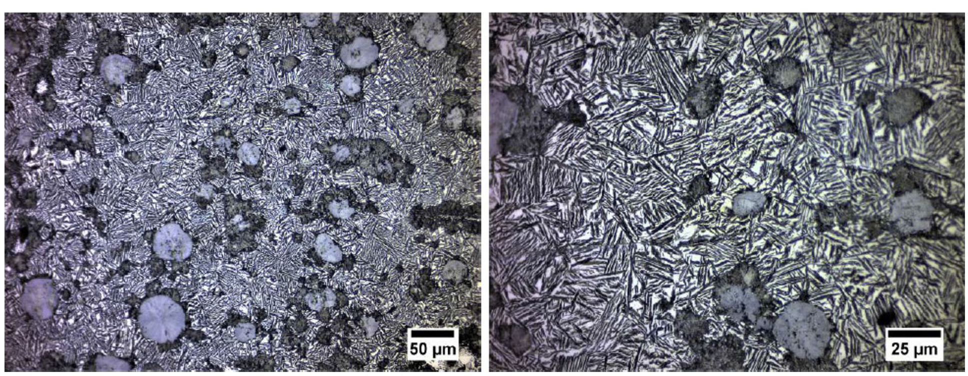

Fig. 8 OM images of microstructure of alloying cast iron austempered at 320 °C with different magnifications (alloying 320)

austempered cast iron is due to the formation of lower bainite and martensitic microstructure. It is noticeable that the hardness decreases by increasing the temperature of austempering to 340 °C. The reason for this phenomenon is the thickening of the acicular ferrite and the formation of residual austenite. By increasing the austempering temperature to 370 °C, the hardness increases up to 470 BHN. This is due to the residual austenite conversion at this

Table 3 Mass loss variation of different specimens after 300 m sliding distance in pin-on-disk test

Specimen	Mass loss after 300 m sliding distance (mg)
GGG60	934
Alloying	79.01
ADI 320	20.32
Alloying 320	5.03

temperature. By this reaction, the carbon-rich residual austenite is converted into ferrite and carbide, in which the carbide, at the boundary between the two phases of austenite and the ferrite, forms continuous phase. The presence of a continuous carbide phase at the interface of phases increases the hardness and brittleness of the cast iron [25].

By comparing the hardness, for selecting the optimum austempering temperature from the hardness curve (Fig. 5), there is a possibility that the toughness of cast iron decreases at 370° C, as it has the highest hardness at this temperature. On the other hand, at 270 °C, it seems the specimen does not have a good ductility due to the lack of residual austenite (Fig. 4a). As a result, the optimum austempering temperature is 320 °C, which is between 300 and 340 °C.

One of the challenges of the austempering of impeller is its low hardenability due to the lack of alloying elements in chemical composition. In other words, in ductile cast iron GGG 60, it is difficult to capture the bainite phase in impeller blades that are very thick because of its low alloying elements (Table 2). Therefore, in order to facilitate the formation of bainite phase in ductile cast iron GGG 60 at thick sections, the hardness of the cast iron needs to be increased.

In general, for the austempering process, ductile cast iron with a thickness of more than 19 mm requires the addition of alloying elements. The presence of alloying elements reduces the possibility of pearlite formation and increases hardenability. The presence of soluble alloying elements causes the tip of the temperature–time–transformation curve to move to the right and the formation of pearlite is delayed. Therefore, the presence of alloying elements of nickel, copper and molybdenum, in ductile cast iron with high thickness, seems to be vital [26, 27].

Also, the presence of molybdenum in the chemical composition leads to the formation of fine carbides that increase the hardness of the cast iron. Figure 6a, b shows microstructures of the alloying cast iron (alloying specimen) after casting, and the chemical composition of the specimens is given in Table 2. It is observed that the graphite is completely spherical and the nodule percentage is about 85% and the matrix is almost perlite. In addition, the graphite morphology of alloying and non-alloying cast iron is according to ASTM A247 standard in groups I and II. It is also clear that spherical graphite, in alloying cast iron, is surrounded by lower ferrite, and so-called bull's-eye structure is not formed. This is due to the presence of alloying elements such as molybdenum and chromium, which results in the formation of intercellular carbides among graphite nodules that spontaneously increase wear/erosion resistance [28]. The EDS analysis of marked spot (given in Fig. 6b) is presented in Fig. 6c. EDS spectrum shows high concentration of Mo and Cr, showing that the marked spot is molybdenum–chromium carbides. Figure 7 shows elemental mapping of alloying elements, which is in accordance with the presented EDS results. Figure 8 shows the microstructure of alloying cast iron austempered at 320 °C, and the presence of an ausferrite microstructure is quite clear.

3.3 Wear and Mechanical Properties

In Table 3, mass loss based on the sliding distance, in the wear test for the initial ductile iron (failed impeller), after the austempering process at 320 °C (ADI320), raw alloying cast iron and alloying cast iron austempered at 320 °C (Alloying 320) is compared.

It is observed that the amount of mass loss of the initial ductile cast iron increases about 45 times compared to the austempered cast iron during 300 m sliding distance. This sharp increase in the war resistance of ADI320 cast iron is

Table 4 Comparison between some mechanical properties of primary ductile cast iron and alloying cast iron, after and before austempering process

Specimen	UTS (MPa)	Hardness (BHN)	Elongation (%)	Impact toughness (J) (without notch)
Primary ductile cast iron	609	260	5.5	55
Alloy	682	277	4.4	28
ADI 320	920	320	3.5	40
Alloying 320	1020	375	2.2	–

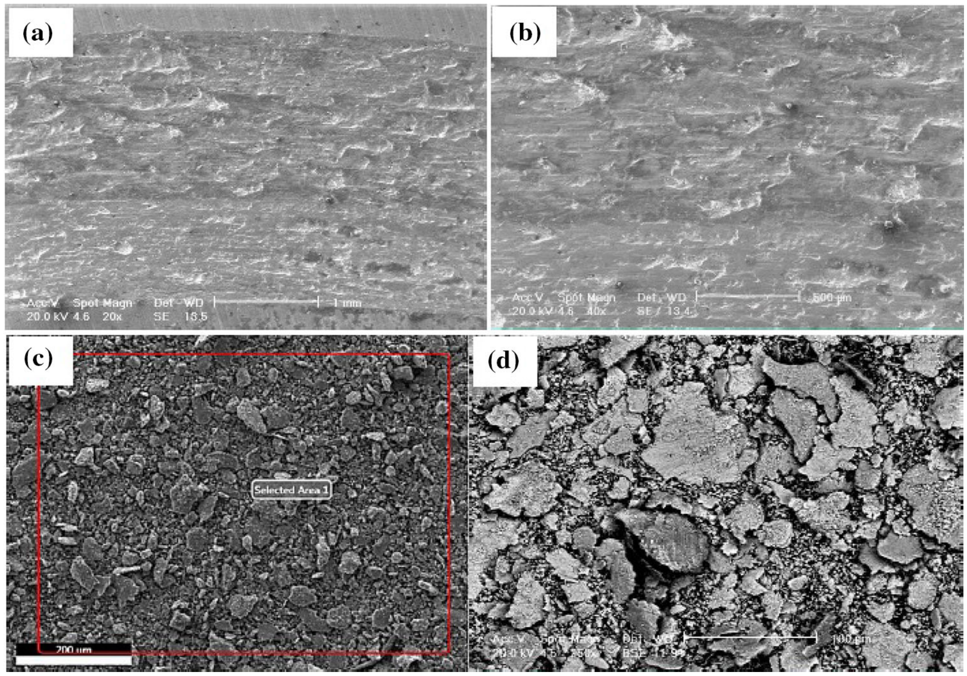

Fig. 9 SEM micrographs of alloying sample: **a** and **b** worn surface; **c** and **d** wear debris morphologies

due to the presence of low bainite zone with acicular ferrite and carbon-rich residual austenite. The presence of austenite in the microstructure improves the wear resistance. The residual austenite transforms to martensitic, while stress is applied [18, 23].

The formation of the martensitic phase at the surface causes a higher wear resistance, due to the higher hardness than austenite, which is a type of surface modification. It is important that wear resistance of alloying cast iron increases, compared to primary cast iron, which is due to the presence of carbides. This is also true for increase in the abrasion resistance of cast alloy castings to conventional cast iron castings. Additionally, the hardness is inversely related to the mass loss phenomenon [28].

On the other hand, as shown in Table 4, the hardness of the cast iron alloy is higher than the other specimens, which results in a lower weight loss than other samples. Figures 9, 10 illustrate the SEM micrographs of the worn surfaces of the alloying and alloying 320 samples tested under a load of 120 N for 300 m. There are evidences of metal flow and plastic deformation on the worn surface of alloying samples (Fig. 9a, b), whereas Fig. 9c, d shows the wear debris of alloying specimens. As indicated, debris has a flake-like shape and coarse particles, implying that alloy specimens deform plastically during sliding. According to the morphology of worn surface, it seems that the adhesive mechanism is the dominating wear mechanism.

Figure 10 shows the worn surface and wear debris of Alloying 320 samples. The worn surface exhibits narrow grooves along the direction of sliding, without any plastic deformation. Comparing Figs. 9a and 10a confirms that wear mechanism transforms to abrasive mechanism. Also, wear debris (see Fig. 10c, d) are finer than wear debris of alloying sample.

All of these evidences indicate that abrasive wear is major mechanism and wear resistance is dramatically improved which confirms the results in Table 3. It is noticeable that debris are agglomerated and rounded to oxide particles as shown in Fig. 10c, d; the EDS analysis, from oxide particles, is shown in Fig. 10e. The formation of oxide particle debris is a result of oxidative wear; hence, the alloying 320 samples have the highest wear resistance. Also, the appearance of oxide particles can be attributed to decrease in of the wear rate of alloying 320 samples [29, 30].

A comparison of the mechanical properties of primary ductile cast iron with other specimens is given in Table 4. The ultimate tensile strength is noticeably observed in the alloying 320 sample because the formation of matrix consists of acicular ferrite with carbide. The highest elongation (5.5%) is recorded for primary ductile cast iron, due to the presence of ferrite around the graphite spheres.

However, it is known that with the austempering process, the UTS increases, so elongation % and impact toughness decrease. The reduction in elongation and impact toughness due to the austempering process may destroy the impeller blades during operation time.

In fact, the impeller blade is damaged due to the rotation of the fan blade around the central axis and its elastic deformation occur during operation in a sieve, and this elastic deformation exceeds its permissible limit. Therefore, the working conditions of the blades are simulated to

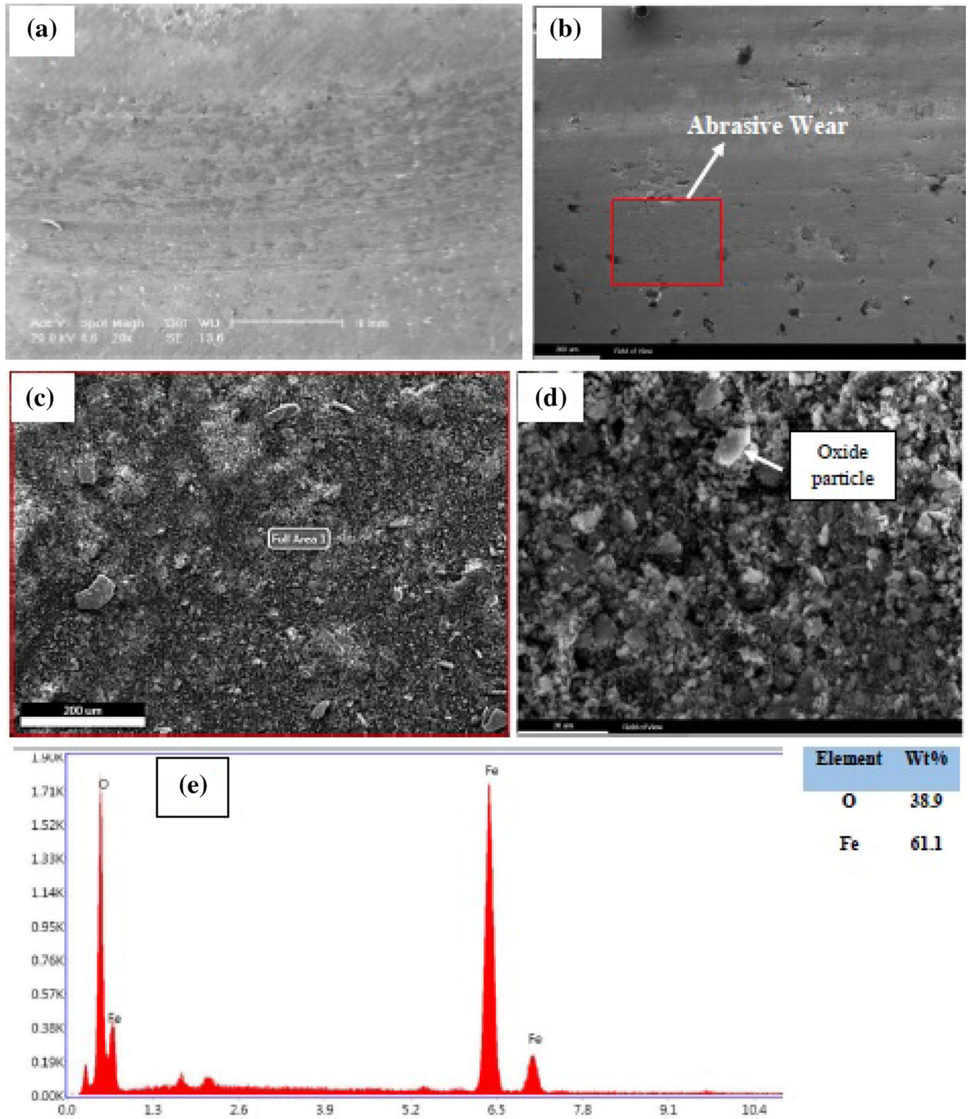

Fig. 10 SEM micrographs of the alloying 320 sample: **a** and **b** worn surface; **c** and **d** wear debris **e** EDS analysis of oxide particle

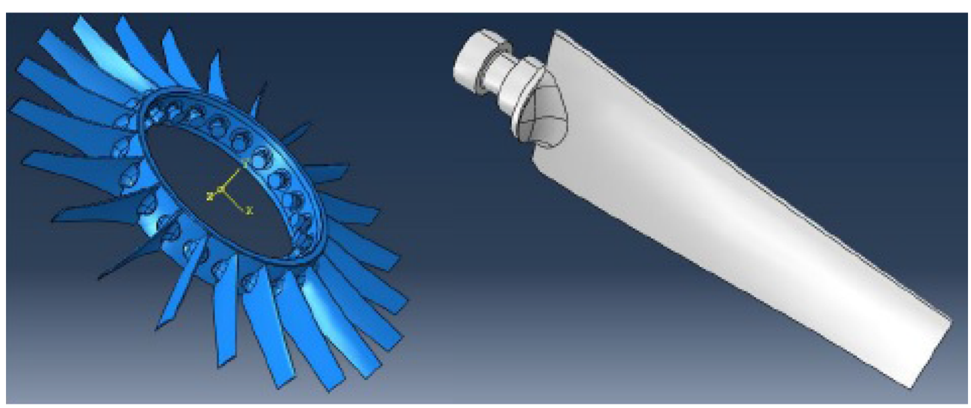

Fig. 11 3D simulation of the fan impeller blade

ensure the proper operation of the blade due to the reduced elongation owing to the austempering process. For this purpose, the geometry of fan blades is depicted by the SolidWorks software shown in Fig. 11.

For modeling of the fan impeller blades, an elastic ductile cast iron model has been used, where the Young modulus and Poisson's ratio are 165 GPa and 0.3, respectively. Since the temperature of the working environment

Fig. 12 Distribution of force applied to fan impeller blades

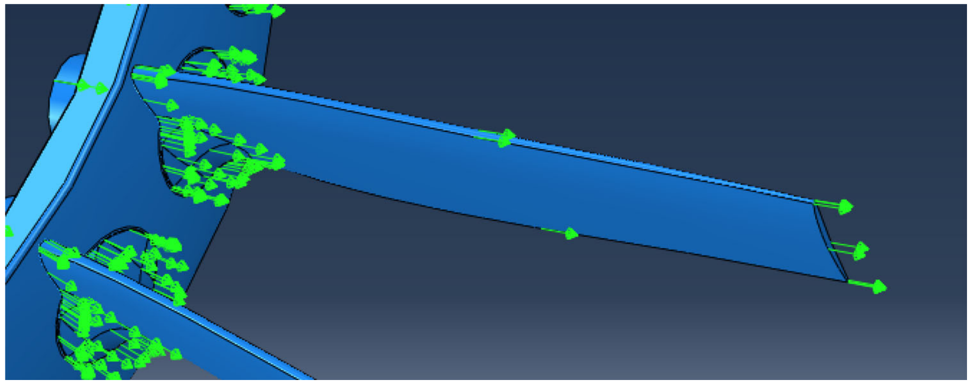

of the fan blades is not high (< 120 °C), the temperature parameter has been discarded from calculations. In order to solve the equilibrium equations, stable and secure solution must be considered. For this purpose, the static general method is used to solve stable problems. Since the rotational speed is constant (435 rpm), it is presumed that equations are independent of time and stability. Therefore, the only external force applied to the system is the one due to the rotation that varies with the rotation speed.

For this purpose, a constant rotation speed has been considered and the value of this force has been calculated and applied to the systems shown in Fig. 12. Depending on the position of exhaust fan, the weight force is aligned with the axis of rotation, and this force is not very effective in comparison with other forces and its effect is negligible.

Also, all degrees of freedom of the collection are restrained apart from rotation. In addition, since this system consists of several interactive species, the interaction between the parts must be specified; therefore, "Tie" constraint type in ABAQUS software selected for the sake of assumption.

For resolving the finite element problems, it is necessary that the domain of solution problem is meshed. For this purpose, the second-order element containing 10 nodes of the tetrahedron element family has been used. Given the fact that the contact between the parts of this set is high, the choice of this element seems to be reasonable. The meshing is also tweaked at more sensitive points such as the edge of the blades, so that the solution can be obtained with proper precision and efficiency. Figure 13 shows a networked fan impeller. In total, 1,018,476 nodes and 604,949 networking elements are used to resolve the entire set.

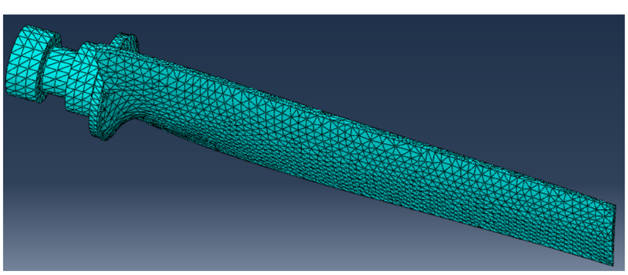

Fig. 13 Meshed geometry of 3D model for one of the blades of the fan impeller

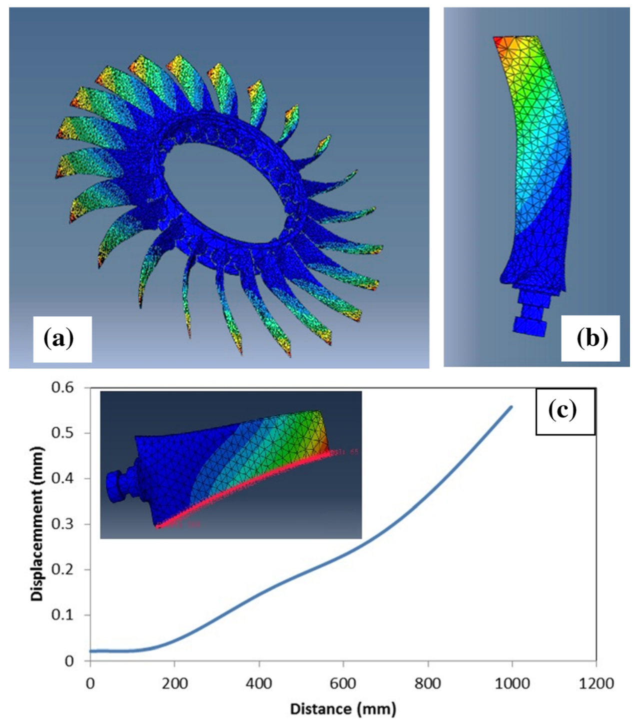

Fig. 14 Displacement distribution of different points of impeller fan blades. **a** Entire system, **b** one of the blades, **c** displacement values with distance variation from tip of impeller fan blades

The solvable model is shown in Fig. 14a, where the displacement of the entire collection is shown. Since the degree of deformation of the impeller blade has higher priority, the solved model of one of the blades is presented in Fig. 14b. Therefore, it is observed that the maximum displacement occurs at the tip of the blade and its value is about 0.5 mm (equal to a strain of about 0.001). Figure 14c shows the value of displacement along the blade: the marked red line along the impeller.

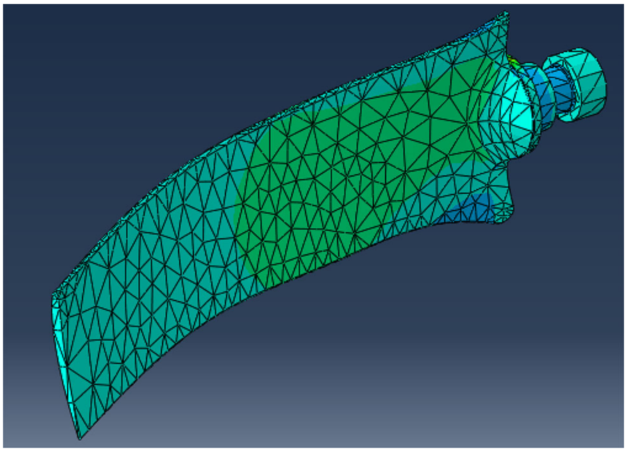

Fig. 15 Service stress distribution in different points of fan blades

Figure 15 shows the distribution of stress on the turbine blade. The maximum stress on the blade is at its prime points, approximately 60 MPa, which is very low compared to its yield limit. Therefore, it can be concluded that the reduction in austempered ductile cast iron GGG60 from 5.5 to 2.2% cannot be really critical and dangerous for the systems.

4 Conclusions

The failure of the impeller fan blades, made of the GGG60 ductile cast iron for the indurating machine of pelletizing plant, was investigated in detail. It was confirmed that as the austempering temperature increased, the residual austenite increased in the microstructure; also, by increasing the temperature of austempering to 340 °C, hardness decreasesd from 439 to 348 HB, due to the increase in the austenite value.

The austempered alloying specimens had the highest wear resistance and the mode of wear was abrasive and oxidative and debris were agglomerated and rounded oxide particles, and therefore, the mass loss value of the abrasion test in austempered alloying cast iron was decreased from 934 to 5 mg compared to primary cast iron. The highest hardness and UTS of the austempered alloying cast iron were achieved as follows: 375 HB and 1020 MPa, respectively; however, the lowest reduction percentage at alloying 320 was determined to be 2.2%.

Considering the simulated working conditions, the maximum stress and displacement of impeller fan blade were 60 Mpa and 0.5 mm, respectively. This work highlights the important parameters to improve the mechanical properties and wear resistance of such alloys in steel industry.

1. As the austempering temperature increased, the residual austenite increased in the microstructure.
2. By increasing the temperature of austempering to 340 °C, hardness decreased from 439 to 348 HB, due to the increase in the austenite value.
3. The mass loss value of the abrasion test in austempered alloying cast iron decreased from 934 to 5 mg compared to primary cast iron.
4. The austempered alloying specimens had the highest wear resistance and the mode of wear was abrasive and oxidative and debris were agglomerated and rounded oxide particles.
5. The highest hardness and UTS of the austempered alloying cast iron were obtained as 375 HB and 1020 MPa, respectively. In addition, the lowest percentage of reduction for alloying 320 was 2.2%.
6. The maximum stress and displacement of fan impeller blade in terms of simulated working conditions were obtained as 60 MPa and 0.5 mm, respectively.

Acknowledgement We are immensely grateful to Mr. Reza Esmaeilpour and Farhang Dabaghnia from Pelletizing Unit, Mobarakeh Steel Company, for their technical support.

References

1. Zhang C, Fu H, Lin J, and Lei Y, *Trans Indian Inst Met* **72** (2019) 1231.
2. Sarkar T, Mukherjee M, and Pal T K, *Trans Indian Inst Met* **71** (2018) 1455.
3. Kawatra S K, and Ripke S J, *Int J Mineral Process* **72** (2003) 429.
4. Zhou Y, Zhang Y, Li G, Wu Y, and Jiang T, *Powder Technol* **271** (2015) 155.
5. Eisele T, and Kawatra S, *Miner Process Extr Metall Rev* **24** (2003) 1.
6. Forsmo S, Forsmo S E, Björkman B, and Samskog P O, *Powder Technol* **182** (2008) 444.
7. Sivrikaya O, and Arol A, *Int J Miner Process* **123** (2013) 158.
8. Kusmonoa K, *Case Stud Eng Fail Anal* **9** (2017) 71.
9. Ariely S, and Khentov A, *Eng Fail Anal* **13** (2006) 925.
10. Liu W, *Eng Fail Anal* **36** (2014) 253.
11. Hayrynen K, Keough J, and Pioszak G, *AFS Trans* (2010) 1.
12. Aristizabal R E, *Intercritical Heat Treatments in Ductile Iron and Steel*, University of Alabama at Birmingham, Graduate School (2012).
13. Hemanth J, *J Mater Process Technol* **101** (2000) 159.
14. Khouzani M K, Bahrami A, and Eslami A, *Eng Fail Anal* **90** (2018) 168.
15. Panda R K, *Effect of Copper on Austempering Behavior of Ductile Iron*, Master of Technology, Department of Metallurgical and Materials Engineering, National Institute of Technology, Rourkela (2011).
16. Toktas G, Tayanc M, and Toktas A, *Mater Charact* **57** (2006) 290.
17. Zimba J, Simbi D, and Navara E, *Cem Concr Compos* **25** (2003) 643.
18. Xu L, Wei S, Xiao F, Zhou H, Zhang G, and Li J, *Wear* **376–377** (2017) 968.

19. Liu F, and Zhou K C, Mater Trans **53** (2012) 1203.
20. Abdou S, Elkaseer A, Kouta H, and Abu Qudeiri J, *Adv Mech Eng* **10** (2018) 1.
21. Mitelea I, Bordeaşu I, Pelle M, and Crăciunescu C, *Ultrason Sonochem* **23** (2015) 385.
22. Abboud J H, *Mater Des* **35** (2012) 677.
23. Khouzani M K, Bahrami A, and Mehr M Y, *J Alloys Compd* **782** (2019) 461.
24. Liu J H, Li G L, Zhao X B, and Hao X Y, Zhang J J, *Effect of Austempering Temperature on Microstructure and Properties of Carbidic Austempered Ductile Iron*, Advanced Materials Research, Trans Tech Publ, 2011, pp. 1085–1088.
25. Eric O, Sidjanin L, Miskovic Z, Zec S, and Jovanovic M, *Mater Lett* **58** (2004) 2707.
26. Hayrynen K L, *The Production of Austempered Ductile Iron (ADI)*, World Conference on ADI (2002), pp. 1–6.
27. Bahrami A, Khouzani M K, Mokhtari S A, Zareh S, and Mehr M Y, *Metals* **9** (2019) 801.
28. Refaey A, and Fatahalla N, *J Mater Sci* **38** (2003) 351.
29. Bahrami A, Anijdan S H M, Golozar M A, Shamanian M, and Varahram N, *Wear* **258** (2005) 846.
30. Mohan S, Prakash V, and Pathak J P, *Wear* **252** (2002) 16.